Multifunctional eco-friendly synthesis of ZnO nanoparticles in biomedical applications

Amal Mohammed Al-Mohaimeed, Wedad Altuhami Al-Onazi, Maha Farouk El-Tohamy*

Department of Chemistry, College of Science, King Saud University, P.O. Box 22452, Riyadh 11495, Saudi Arabia. muhemeed@ksu.edu.sa, woalonazi@ksu.edu.sa moraby@ksu.edu.sa

Corresponding author Amal Mohammed Al-Mohaimeed, Email: muhemeed@ksu.edu.sa,

Abstract

This study describes an eco-friendly synthesis of ZnO nanoparticles using aqueous oat extract. The advanced electrochemical and optical features of green synthesized ZnONPs displayed excellent antibacterial activity, and exhibited an important role in pharmaceutical determinations. The formation of nanoscale ZnO was confirmed using various spectroscopic and microscopic investigations. The formed nanoparticles were found to be around 100 nm. The as-prepared ZnONPs were monitored for their antibacterial potential against different bacterial strains. The inhibition zones for ZnONPs were found as *E. coli* (16 mm), *P. aeruginosa* (17 mm), *S. aureus* (12 mm) and *B. subtilis* (11 mm) using 30 µg mL^{-1} sample concentration. Also, ZnONPs exhibited significant antioxidant effects 58 to 67 % with an average IC_{50} value of 0.88 ± 0.03 scavenging activity and 53 to 71 % (IC_{50} value 0.73 ± 0.05) against the DPPH and ABTS scavenging free radicals, respectively. The photocatalytic potential of ZnONPs for Rhodamine B dye degradation dye under UV irradiation was performed. The photodegradation process was carried out as a function of time-dependent and the complete degradation (nearly 98 %) with color removal after 120 min. Conclusively, the synthesized ZnONPs using oat biomass might provide a great promise in the future for biomedical applications.

 doi:10.20944/preprints202112.0259.v1

Keywords: Oat extract; Zinc oxide nanoparticles; Green synthesis; Antibacterial; Antioxidant; Pharmaceutical analysis.

1. Introduction

Nanoscale materials, especially metal oxide nanoparticles are considered as a distinctive group of materials with unique physicochemical properties and possess broad applications in various scientific areas such as sensing technology [1, 2], cell adhesion and tissue engineering [3], industrial packaging [4, 5] catalysis [6, 7] and biomedical investigations [8, 9].

Zinc oxide nanoparticles (ZnONPs) are among all metal oxide nanoparticles, which have received extensive attention for their advanced biocompatible feature and high strength under utmost circumstances [10, 11]. ZnONPs have been used in medicine [12], sensors [13], industrial additives [14], photocatalysis [15], antioxidants and antibacterial potentials [16, 17].

Conventional methods for the synthesis of ZnONPs need hazardous chemicals with high quantity of extrinsic heat and also produces various harmful side by-products that could possess effective biological and environmental threat. Therefore, there consistently exists a huge require to progress eco-friendly compatible, profitable, energy efficient green chemical methods to avoid the use of toxic materials in the synthesis of nanoparticles [18].

To defeat these drawbacks, natural substances (marine algae, sponges and plants) display the excellent potential resources suitable for the biogenic preparation of metal and metal oxide nanoparticles. The superiority of using plant biomasses in the synthesis of ZnONPs is simple accessibility, eco- friendly and mostly safe [19]. These plants contain various types of biomolecules such as phenolic compounds terpenoids, carboxylic acids, alkaloids that can potentially serve as reducing and stabilizing agents

Preprints (www.preprints.org) | NOT PEER-REVIEWED | Posted: 15 December 2021 doi:10.20944/preprints202112.0259.v1

in the preparation of metal oxide nanostructures [20]. The oat (*Avena sativa*) is a type of cereal grain belongs to the plant family *Poaceae grass*. The grain refers particularly to the edible seeds of oat grass, which is approved by the Food and Drug Administration as healthy food labels correlating a reduced risk of various diseases including coronary heart disease and diabetes. Oat grains also used in weight control and digestive health [21-24]. Literature survey claims that *A. sativa* extract contains macromolecules such as phenolic compounds, amino acids, carotenoids, proteins, starch and unsaturated fatty acids [25]. These biomolecules over the above-described medicinal properties exhibit antimicrobial and antioxidant activities [26, 27]. Besides, the phytochemical profile of oat biomass includes natural chemical components which have been utilized for the biosynthesis of nanoparticles such as metal and metal oxide nanoparticles [28, 29]. Additionally, one of the major environmental hazards is the effluent from the dyeing and pigment industries which possess various toxic and non-biodegradable by-products [30]. A water-soluble xanthene dye (Rhodamine B, RB) is one of the common dyes that widely used in various industrial applications such as plastic dying, as a trace dye for determining the water rate flow and direction, textile industry pharmaceuticals and cosmetics. This dye is considered as one of the most organic environmental pollutant [31].

Photodegradation of organic pollutants to less harmful wastes can be considered as an effective method to minimize the huge quantity of industrial waste materials being liberated into the environment [32]. Various conventional techniques including, spectroscopy, chromatography and chemical oxidation have been addressed in different industries for dyes bleaching [33]. Additionally, few recent techniques include, solar photofenton, photobiological degradation and sonochemical degradation have been reported for dyes removing [34-36]. Nevertheless, these techniques possess certain

Preprints (www.preprints.org) | NOT PEER-REVIEWED | Posted: 15 December 2021 doi:10.20944/preprints202112.0259.v1

downsides such as high energy consumption, high cost, and complicated instrumentation. Also, they consume large amounts of toxic chemicals. Therefore, it is important to suggest simpler, facile and less environmental pollutant approach to remove these toxic dyes from industrial waste products. Recently, nanoscience research has been concerned with using green nanotechnology in the biosynthesis and characterization of metal oxide nanoparticles for potential photocatalytic activity.

Zinc oxide nanoparticles have astonishing biomedical applications and are included in ointments used for the treatment of wounds, heart burns, and bone regeneration [37]. Moreover, ZnONPs have exhibited excellent toxic potentials against different multidrug resistant human microorganisms and can be recommended as an alternative medication [38]. Also, ZnONPs with their unique optical and catalytic features are designed as photochemical degradation nanomaterials [39].

Considering the medicinal importance of metal oxide nanoparticle synthesis, especially ZnONPs using plant biomasses, the aim of the present study was eco-friendly synthesis and characterization of ZnONPs using oat biomass as natural reducing agents. The biomedical potential of the prepared ZnONPs was separately investigated for antibacterial, antioxidant and photocatalytic properties.

3. Results and discussion

3.1. Characterization of green synthesized ZnONPs

The formation of ZnONPs was characterized using various spectroscopic techniques. UV-Vis spectroscopy was applied to study the optical properties of the as-prepared ZnONPs. The absorption spectrum showed a clear broad absorption peak at 374 nm for ZnONPs (Figure 1a). The change of oat biomass color from yellowish to pale white after boiling for 20 min then to white after heating at 500º C for 2 h might be attributed to the photo excitation of surface plasmon vibrations from the valence band to the

Preprints (www.preprints.org) | NOT PEER-REVIEWED | Posted: 15 December 2021 doi:10.20944/preprints202112.0259.v1

conduction band of the formed ZnONPs [40]. These color changes revealed the complete interaction of oat biomass and zinc nitrate hexahydrate producing ZnONPs. The band gap of the synthesized ZnONPs was calculated using following formula:

$$Eg = h\upsilon = hc/\lambda \quad (4)$$

Where, h, c and λ are Planck's constant (6.626×10^{-34} J s), the velocity of light (3×10^{8} m/s) and the wavelength (nm), respectively. The band gap of was found to be 3.61 eV at wavelength (λ_{max} 374 nm) which is confirmed the formation of nanoparticles when compared with the band gap of ZnO bulk (3.3 eV). The optical outcomes of ZnONPs were matched those previously reported [41]. Moreover, in nano materials, the relation between the size diameter of the particles and the band gap is inversely proportional to each other. The decrease in band gap the increase in nanoparticles in size diameter, due to quantization effect, but it never reaches zero [42].

Photoluminescence (PL) detection was used to determine the emission properties of ZnONPs (Figure 1b). The photoluminescence of ZnONPs sample showed five significant emission bands at 403, 445 and 470 nm (blue bands), 485 (green band) and 530 nm (red bands). The three blue bands are correlated to the defect structures in ZnO crystal. However, the two green and red bands can be correlated to the transition between the oxygen vacancy and interstitial oxygen [43]. FT-IR spectrum was recorded to study the possible existence biomolecules responsible for the reduction and capping of the green synthesized ZnONPs. The particular vibration bands were identified from the wave numbers range 4000-400 cm^{-1}. The FT-IR spectra of oat biomass before and after the reaction of zinc nitrate hexahydrate to ZnONPs were shown in Figures 2a and 2b. The FT-IR spectrum of oat biomass showed various absorption bands at 3754 (medium O-H stretching), 3430 (strong O-H stretching), 2925 (C-H stretching) [44], 2350 (medium N-H amine II), 1633 (strong C=C alkene), 1405 (symmetric stretching

Preprints (www.preprints.org) | NOT PEER-REVIEWED | Posted: 15 December 2021 doi:10.20944/preprints202112.0259.v1

carboxyl side groups of amino acids residue), 1261 (amide III band of protein) [45], 1030 (C–N stretching vibration of amine) and 620 cm^{-1} (strong C-halo, alkyl halide). The previous observed bands have been shifted to be at 3750, 3424, 2922, 2348, 1625, 1383, 1126, 1028, 445 (Zn-O band) cm^{-1} in ZnONPs sample [43]. The recorded results confirmed that the synthesized ZnONPs were surrounded by the metabolites of biomolecules such as tocopherols and tocotrienols, phenolic acids, carbohydrates, phenolic alkaloids (avenanthramides). The carbonyl groups of the amino acid residues and proteins have the stronger ability to bind with metal oxide ions indicating their reduction of zinc nitrate to Zn-O and also acted as capping the resulted nanoparticles.

XRD analysis was also performed to evaluate the crystalline structure and phase purity of the green synthesized ZnONPs using (K_α radiation (λ = 1.5418 Å), operating current 30 mA and voltage 35 kV) at scan rate 0.3 s/ point and 0.02° resolution at room temperature. The XRD pattern displayed various significant peaks at 31.13° (1 0 0), 34.53° (0 0 2), 37.22° (1 0 1), 47.67° (1 0 2), 57.18° (1 0 3), 63.07° (2 0 0), 68.21° (2 0 2) and 72.03 (0 0 4) orientation, respectively (Figure 2c). The diffractogram showed an excellent matching with the hexagonal phase (wurtzite structure) when compared with the results of JCPDS card No. 89-1397 and no impurity peaks were observed. The average particle size of ZnONPs sample was calculated using Scherer's equation:

$$D = 0.9\lambda/\beta Cos\Theta \quad (5)$$

Where, D is the average crystal size, k is the shape factor (0.9), λ is the wavelength (0.15416), β is the Bragg angle Θ of the X-ray (1.5406 Å) Cu Ka radiation. The average crystallite size of ZnONPs was found around 100 nm.

The EDX analysis was performed to quantify the chemical compositions of the green synthesized ZnONPs using oat biomass. The EDX spectrum showed significant signals corresponding to Zn (weight%, 69.9% and atomic %, 36.2%), O (weight%, 30.1% and

Preprints (www.preprints.org) | NOT PEER-REVIEWED | Posted: 15 December 2021 doi:10.20944/preprints202112.0259.v1

atomic % 63.77%) elements revealing the formation of ZnONPs (Figure 3). The results revealed the presence of metallic zinc oxide with high purity and no any additional peaks corresponding to other elements were recorded.

Microscopic analysis was performed to visualize the size and the surface shape of the synthesized ZnONPs. The size and shape of ZnONPs were demonstrated in Figure 4a. This image revealed that the formed nanoparticles are nano crystalline hexagonal in shape with size distribution around 100 nm. SEM image showed that the clusters of ZnONPs are nearly hexagonal in shape with rough surface and the size around 100 nm (Figure 4b).

3.2. Antibacterial activity

The antibacterial effect of green synthesized ZnONPs with oat biomass was studied and the outcomes confirmed that ZnONPs exhibited excellent antibacterial potential in a dose dependent manner (Table 1). The calculated inhibition zones were found as *E. coli* (16 mm), *P. aeruginosa* (17 mm), *S. aureus* (12 mm) and *B. subtilis* (11 mm) for ZnONPs (Figure 5). Thus, recorded results revealed that the ZnONPs synthesized by oat biomass showed excellent antibacterial potential against all bacterial stains. The highest activity was noticed against *P. aeruginosa and E. coli* by using 30 µg mL^{-1}. Moreover, the higher antibacterial behavior of ZnONPs (oat biomass) can be ascribed to their small particle size, shape as well as the bioactive nature of oat phytochemical components.

3.2.1. Bacteriostatic and bactericidal estimation

Bacteriostatic (MIC) and bactericidal (MBC) of ZnONPs against *P. aeruginosa and E. coli* were studied using agar well diffusion method. The suitable minimum concentration to inhibit the visible growth of *P. aeruginosa and E. coli* was estimated after 24 h incubation time at 37˚C. It was observed that the gradual increase in ZnONPs

Preprints (www.preprints.org) | NOT PEER-REVIEWED | Posted: 15 December 2021 doi:10.20944/preprints202112.0259.v1

concentration from 5 to 640 µg mL^{-1} caused a remarkable reduction in the viability of bacterial cells ($p < 0.05$). The MIC was found as 160 µg mL^{-1} for *P. aeruginosa and E. coli*.

MBC is known as the least concentration of test sample compound can lead to bacterial cell death under a particular condition through a fixed time period [46] (Figure 6a and 6b). The MBC for *P. aeruginosa and E. coli* were 160 and 320 µg mL^{-1} of ZnONPs, respectively (Table 2). The possible mechanism of ZnONPs bactericidal potential can be explained as cell membrane damage due to the oxidative stress produced from the release of free radicals, reactive oxygen species (ROS) and reactive nitrogen species (RNS). Also, the bacterial cell damage can be attributed to the interaction between lipopolysaccarides in the outer membrane of the bacterial cells with Zn^{2+} ions (Figure 7) [47]. The appeared inhibition zones could be assigned to the penetration of ZnONPs to the bacterial cells, causing their growth inhibition and damage.

3.2.2. Morphological changes of bacterial stains under SEM

The morphological changes of *P. aeruginosa* and *E. coli* surface were investigated under SEM. As a result, the cells treated with oat biomass swallowed with slight change in the morphological shape (Figures 8b and 8e). The surface coating of bacterial cells by ZnONPs, showed significant change in the shape of bacterial cells with significant cell damage (Figures 8c and 8f). ZnONPs penetrate the peptidoglycan membrane of *P. aeruginosa and E. coli* leading to its damage, releasing the cell contents and consequently leading to cell death [47]. These results were compared with control (untreated bacterial cells) (Figures 8a and 8d).

3.3. Antioxidant activity of ZnONPs

The influence of various concentrations of ZnONPs and Oat biomass on DPPH free radical antioxidant potential was presented in Table 3. The data showed that both

Preprints (www.preprints.org) | NOT PEER-REVIEWED | Posted: 15 December 2021 doi:10.20944/preprints202112.0259.v1

ZnONPs and oat biomass have free radical scavenging activity. However, the synthesized ZnONPs exhibited stronger scavenging activity against DPPH than oat biomass. The DPPH potential of ZnONPs and oat biomass was observed to elevate in a dose dependent manner. At the concentrations 25-100 μg mL^{-1}, the green synthesized ZnONPs showed 58 to 67 % with an average IC_{50} value of 0.88 ± 0.03 scavenging activity. The antioxidant activity was lower than that of ascorbic acid at 100 μg mL^{-1} (73 %). Furthermore, in ABTS assay, the ability of ZnONPs to reduce ABTS to $ABTS^{+}$ ions were also notably higher than the oat biomass at different concentrations from 25 to 100 μg mL^{-1} by 53 to 71 % (IC_{50} value 0.73 ± 0.05). The outcomes of this study revealed that oat biomass is an excellent source of phenolic compounds, which are the most important secondary metabolites responsible for antioxidant activity. Also, the tunable physical and chemical properties of ZnONPs showed significant antioxidant activity.

3.4. Photocatalytic effect of ZnONPs

The photocatalytic effect of the green synthesized ZnONPs to produce RB degradation was investigated in aqueous solution under a visible irradiation. The degradation of the RB was determined with UV/Vis absorption spectra by measuring the intensity of the absorption maxima peak at 550 nm against the irradiation time. The photodegradation of RB dye was increased with time and the complete degradation was achieved nearly (98 %) with decolorization after 120 min (Figure 9). The outcomes of the current study provided an excellent catalytic potential of the green synthesized ZnONPs towards the reductive degradation of RB dye and the results were in agreements with the previously reported studies [48]. A linear relationship (Beer's-Lambert law) was obtained from plotting concentrations of RB against the absorption maxima at 550 nm. This can be ascribed to the stable number of photons present for photodegradation. The capping

Preprints (www.preprints.org) | NOT PEER-REVIEWED | Posted: 15 December 2021 doi:10.20944/preprints202112.0259.v1

layer of reducing agent (oat biomass) on ZnONPs surface may also enhance the potential adsorption between ZnONPs and RB molecules. Consequently, the redox reaction between RB and reducing agent can be displayed more rapidly for nanoscale particles [49]. The obtained results revealed that the high reactivity of large surface area of ZnONPs provided an efficient photocatalysis for dye degradation under UV light and confirmed that ZnONPs are suitable to reduce and eliminate the hazardous dye pollution. The possible reduction-oxidation mechanism can be represented as follow:

$RB/ZnO + h\nu \; RB\ (visible\ light) \rightarrow RB^*/ZnO$ (6)

$RB^*/ZnO \rightarrow RB^+/ZnO + e^-$ (7)

$e^- + O_2 \rightarrow O_2^-$ (8)

$H_2O + O_2^- \rightarrow {}^{\circ}OOH + OH^-$ (9)

$2\,{}^{\circ}OOH + O_2 \rightarrow H_2O$ (10)

${}^{\circ}OOH + H_2O + e^- \rightarrow H_2O_2 + OH^-$ (11)

$H_2O_2 + e^- \rightarrow {}^{\circ}OH + OH^-$ (12)

$H_2O_2 + {}^{\circ}O_2^- \rightarrow {}^{\circ}OH + OH^- + O_2$ (13)

The generation of electron hole pair resulted from the transfer of excited electrons from the valance band to the conduction band explains the mechanism of photocatalysis in dye under irradiation. The dye molecules were oxidized to non-toxic products (water, carbon dioxide, etc.) due to the formation of hydroxyl radicals. The high stability, conductivity and unique optical features of ZnONPs enable a suitable trapping of photoexcited electrons on their surface and prevent the recombination of electron hole recombination [50]. Moreover, the photocatalysis of ZnONPs under visible light can be produced due to the surface plasmon resonance, the generation of free radicals and interaction with oxygen molecules resulted from the collective oscillations of electrons.

Preprints (www.preprints.org) | NOT PEER-REVIEWED | Posted: 15 December 2021 doi:10.20944/preprints202112.0259.v1

Additionally, the formation of positive holes conducted from electron excitation resulted in the degradation of RB dye [51].

2. Materials and Methods

2.1. Collection of oat biomass

After oat seeds harvest, oat biomass was collected and cleaned by washing thoroughly with tab water then dried at 80 ºC for 12 days to eliminate the residual moisture. The obtained oat biomass was further grinded using electric grinder (Vermeer, model-HG-200) and sieved using a stainless-steel fine mesh sieve to obtain a homogenous powder.

2.2. Chemicals and reagents

All chemicals used in this study were of high pure analytical grade. Zinc nitrate hexahydrate, dimethylsulfoxide (DMSO), ascorbic acid, osmium tetroxide, glutaraldhyde, phosphate buffer saline, ethanol, methanol, potassium persulfate, 2,2-diphenyl-1-picrylhydrazyl (DPPH) and 2,20 -azino-bis [3-ethyl benzo thiazoline-6-sulphonic acid] (ABST) were purchased from Sigma-Aldrich (Hamburg, Germany).

2.3. Bacterial strains and nutritional matrices

All bacterial stains included in this study were provided by Microbiology Department, King Saud University, Saudi Arabia. The *Escherichia coli* (ATCC 25966), *Pseudomonas aeruginosa* (ATCC 27853), *Staphylococcus aureus* (ATCC 25923) and *Bacillus subtilis* (ATCC 6633) were used as Gram negative and positive bacteria. To pre-culture of these isolates was performed using nutrient agar (Oxoid).

2.4. Preparation of aqueous oat biomass extract

The aqueous extract of oat biomass was prepared by mixing 20 g of dried oat powder with 200 mL distilled water and boiled at 100 ºC for 1h. After cooling at room

Preprints (www.preprints.org) | NOT PEER-REVIEWED | Posted: 15 December 2021 doi:10.20944/preprints202112.0259.v1

temperature, the obtained extract was filtered using Whatman filter paper No. 40 and stored in a refrigerator at 4 ºC.

2.4. Preparation of ZnONPs using oat biomass extract

The green synthesis of ZnONPs was conducted by mixing 5.0 g of zinc nitrate hexahydrate with 50 mL oat extract (yellowish in color) in a measuring flask and stirred continuously under magnetic stirring on a hot plate and boiled to 100 °C for 20 min. A pale white precipitate was formed. Then it was calcined at 500 °C for 2 hours. The white ZnO nano powder was obtained and stored in air tight glass container.

2.5. Spectroscopic and microscopic characterization

UV–Vis spectrum was recorded using spectrophotometer (Shimadzu Corporation, Kyoto, Japan) at absorption wavelength range of 200-500 nm for the primary characterization of the synthesized ZnONPs. The Fourier-Transform Infrared spectroscopy (FTIR, PerkinElmer, Waltham, USA) was performed in the IR region of 4000-400 cm^{-1} to study and confirm the possible predictable functional groups. The X-ray diffraction (XRD, Shimadzu XRD-6000 diffractometer, Kyoto, Japan) was also carried out to study the crystalline shape of the synthesized ZnONPs using (Kα radiation (λ = 1.5418 Å), operating current 30 mA and voltage 35 kV) at scan rate 0.3 s/ point and 0.02º resolution at room temperature. The surface morphology of the prepared ZnONPs was examined under scanning electron microscope (SEM, JSM-7610F; JEOL, Tokyo, Japan) and transmission electron microscope (TEM, JEM-2100F, JEOL Ltd, Tokyo, Japan). Furthermore, the elemental content of the synthesized ZnONPs was determined using Energy-Dispersive X-Ray Spectroscopy (EDX, JSM-7610F; JEOL, Tokyo, Japan) in connection with a SEM microscope.

Preprints (www.preprints.org) | NOT PEER-REVIEWED | Posted: 15 December 2021 doi:10.20944/preprints202112.0259.v1

2.6. Antibacterial activity

Antibacterial potential of green synthesized ZnONPs with oat biomass was screened in terms of zone of inhibition using agar well diffusion assay [52] against different bacterial Gram negative; *Escherichia coli* ATCC 25966 and *Pseudomonas aeruginosa* ATCC 27853) and (Gram positive: *Staphylococcus aureus* ATCC 25923 and *Bacillus subtilis* ATCC 6633 strains. The bacterial isolates were pre-cultured on nutrient agar (Oxoid). The bacterial suspension of 0.5 McFarland turbidity of each stain was prepared in 5 mL nutrient broth tubes for the antibacterial study. Sterile cotton swabs were used to load the resulted bacterial suspensions on the surface of Mueller Hinton (Oxoid) plates. Wells (6 mm) were assembled on the surface of the agar plates by using a sterile cork borer and then 100 µL of each ZnONPs (10-30 µgmL^{-1} DMSO) was loaded. The prepared plates were aerobically incubated for 24 h at 37˚C.

2.7. Bacteriostatic and bactericidal estimation

In present assay, minimum inhibitory concentration (MIC) of ZnONPs against *P. aeruginosa and E. coli* and was estimated in triplicates by applying Micro-broth dilution method. The investigated concentrations were taken in the range of 5 to 640 µg mL^{-1}. This assay was conducted by performing 2-fold serial dilutions in 96 well plates. The positive control (Bacterial cells and the broth) was prepared in the first column. The last column (ZnONPs and broth) was considered as the negative control. About 50 µL of each of the bacterial suspensions was loaded and after incubation time (24 h at 37 ˚C) the results were writing down at 600 nm using an ELISA reader (Biotech, Wuxi, China). For matching the results, tetracycline (TE, 25 µg) and DMSO were used as a positive and negative control, respectively. The least concentration of ZnONPs which can lead to a complete bactericidal effect (MBC) was determined by loading aliquots of tubes with first turbid and no visible growth. Amounts of treated samples

Preprints (www.preprints.org) | NOT PEER-REVIEWED | Posted: 15 December 2021 doi:10.20944/preprints202112.0259.v1

were uniformly distributed on nutrient agar plates using a sterile L rod and incubated for 12 h at 37˚C.

2.8. Morphological study of P. aeruginosa and E. coli

The surface morphology of both treated and untreated *P. aeruginosa and E. coli* was investigated under SEM to evaluate the effect of ZnONPs. Prior to examination under microscope, the treated *P. aeruginosa and E. coli* bacteria were cut into pieces (5- by10-mm), fixed in glutaraldehyde in phosphate buffer saline (3 %) solution for 1 h. Then, they fixed in osmium tetroxide (2 %) solution for 1h. The tissues were dehydrated in ethanol and dried with carbon dioxide. To examine under SEM, the dried tissues were loaded on Al stubs with Ag pain vacuum coated with Au-palladium alloy and investigated using SEM at 15 kV acceleration voltage.

2.9. Antioxidants

The antioxidant potential of ZnONPs was determined using two different radical scavenging assays, 2,2-diphenyl-1-picrylhydrazyl (DPPH) and ABTS (2,20 -azino-bis [3-ethyl benzo thiazoline-6-sulphonic acid]). The DPPH free radical scavenging potential of Oat and ZnONPs was evaluated following the standard methods [53]. Prior to the investigation, 1.0×10^{-4} mol L^{-1} DPPH, three different concentrations (25, 50, 100 µg mL^{-1}) of oat and ZnONPs and ascorbic acid (AA) were prepared in menthol. Approximately, 50 µL of DPPH solution was mixed with different concentrations of oat and ZnONPs as well as AA in a 96-well microplate. The prepared mixture was continuously shacked in dark place for 30 min using orbital shaker. The absorbance of the sample was determined using UV–VIS BioTek microplate (Biotech ELx 800; Biotek instruments, Inc, Highland Park, USA) after incubation for 30 min at 518 nm against methanol as blank.

The scavenging ability was calculated using the following equation:

Preprints (www.preprints.org) | NOT PEER-REVIEWED | Posted: 15 December 2021 doi:10.20944/preprints202112.0259.v1

$$\% \text{ DPPH free radical scavenging effect} = C_r - T_r / C_r \times 100 \quad (1)$$

Where, Cr and Tr represent the absorbance of the control and test samples, respectively.

The 2, 20 -azino-bis [3-ethyl benzo thiazoline-6-sulphonic acid]) (ABTS) free radical scavenging assay was also used to evaluate the antioxidant activity of oat extract and ZnONPs using a reported standard method [54]. Briefly, 7.4×10^{-3} ABTS and 2.6×10^{-3} mol L^{-1} of potassium persulfate solutions were separately prepared. The working solution of ABTS was obtained by mixing equal amounts of the previously prepared stock ABTS and potassium persulfate solutions and kept without stirring for 12 h in the dark place. The analysis was conducted by mixing 125 µL of the ABTS working solution with 10 µL of different concentrations (25, 50, 100 µg mL^{-1}) of oat and ZnONPs tested samples as well as ascorbic acid as a control. The final reaction mixture was kept aside for 2 h in dark place. The absorbance of the samples was recorded at 518 nm using UV–VIS BioTek microplate *vs.* methanol as the blank reference. The scavenging potential was calculated using the following equation:

$$\% \text{ ABTS free radical scavenging effect} = C_r - T_r / C_r \times 100 \quad (2)$$

Where, Cr and Tr represent the absorbance of the control the test samples, respectively.

2.10. Photocatalysis

To investigate the photocatalytic potential of the green synthesized ZnONPs, light irradiation using UV chamber (15"×18"×22") with UV lamp (Hamamatsu LC8; lamp power of 0.1 W) was utilized to depredate Rhodamine B (RB) dye at a wavelength 550 nm at ambient temperature. Approximately, 1.0 mg of ZnONPs was mixed with 2.0 mL of RB dye solution (5.0×10^{-6} mol L^{-1}) and sonicated for 5.0 min then kept under constant magnetic stirring for 30 min to ensure an adsorption/desorption equilibrium on the ZnONPs surface prior to irradiation. Under the same conditions a sample with

Preprints (www.preprints.org) | NOT PEER-REVIEWED | Posted: 15 December 2021 doi:10.20944/preprints202112.0259.v1

no ZnONPs was used as a control. Also, the physisorption of ZnONPs surface was evaluated by maintaining the sample in the dark. The detection was conducted by monitoring the samples every 10 min intervals. Briefly, the collected samples were centrifuged at 8000 rpm for 10 min and the supernatant of each sample was measured using UV–Vis spectrophotometer. A Perkin Elmer (Waltham, MA, USA) UV–vis spectrophotometer was used to record the rate of degradation at λ_{max} 550 nm by measuring the reduction in absorption intensity of RB dye. The following equation was used to calculate the degradation efficiency (DE):

$$DE\% = A_0 - A\ A_0 \times 100 \qquad (3)$$

Where, A_0 and A are the initial absorption and absorption intensity after photocatalytic degradation at λ_{max} 550 nm.

Conclusion

The present study suggested clean and simple, safe and cost-effective approach for the green synthesis of ZnONPs using oat biomass. The resulted metal oxide nanoparticles were characterized using various spectroscopic and microscopic techniques to confirm the formation of ZnO nanostructure. The results revealed the preparation of ZnONPs with particles size around 100 nm. The resulted ZnONPs were screened for antibacterial activity and they exhibited high antibacterial potential against different Gram positive and Gram-negative bacterial strains. The green synthesized ZnONPs have shown significant antioxidant activity. The DPPH potential of ZnONPs showed 58 to 67 % with an average IC_{50} value of 0.88 ± 0.03 scavenging activity and in ABTS assay, the ability of ZnONPs to reduce ABTS to $ABTS^+$ ions was 53 to 71 % (IC_{50} value 0.73 ± 0.05). Also, ZnONPs exhibited the highest photocatalytic activity for RB dye degradation (98 %) under visible light irradiation for 120 min.

Author Contributions: Conceptualization, writing and review A. M. A-M; formal analysis, data analysis, W.O.; methodology, validation, and editing visualization M. F. E-T

Funding: This research was funded by Researchers Supporting Project in King Saud University supported this project and the code number is (RSP-2021/247).

Acknowledgments: This study was supported by Researchers Supporting Project number (RSP-2021/247), King Saud University, Riyadh, Saudi Arabia.

Conflicts of Interest: The authors clarified that no conflict of interest in this study.

Data Availability: The data used to support the findings of this study are included within the article.

References

1. Balasubramani, V.; Chandraleka, S.; Rao, T.S.; Sasikumar, R.; Kuppusamy, M.R.; Sridhar, T.M. Recent advances in electrochemical impedance spectroscopy based toxic gas sensors using semiconducting metal oxides. *J. Electrochem. Sci.* **2020**, *167*, 037572. DOI: 10.1149/1945-7111/ab77a0
2. Manjakkal, L.; Szwagierczak, D.; Dahiya, R. Metal oxides based electrochemical pH sensors: Current progress and future perspectives. *Prog. Mater. Sci.* **2020**, *109*, 100635. https://doi.org/10.1016/j.pmatsci.2019.100635
3. Murugesan, B.; Pandiyan, N.; Arumugam, M.; Sonamuthu, J.; Samayanan, S.; Yurong, C.; Juming, Y.; Mahalingam, S. Fabrication of palladium nanoparticles anchored polypyrrole functionalized reduced graphene oxide nanocomposite for antibiofilm associated orthopedic tissue engineering. *Appl. Surf. Sci.* **2020**, *510*, 145403. https://doi.org/10.1016/j.apsusc.2020.145403
4. Ghozali, M.; Fahmiati, S.; Triwulandari, E.; Restu, W.K.; Farhan, D.; Wulansari, M.; Fatriasari, W. PLA/metal oxide biocomposites for antimicrobial packaging

application. *Polym-Plas. Technol. Mater.* **2020**, *59*, 1332-1342. https://doi.org/10.1080/25740881.2020.1738475

5. Basavegowda, N.; Mandal, T.K.; Baek, K.H. Bimetallic and trimetallic nanoparticles for active food packaging applications: A review. *Food Bioproc. Tech.* **2020**, *13*, 30-44. https://doi.org/10.1007/s11947-019-02370-3
6. Juibari, N.M.; Tarighi, S. Metal–organic framework-derived nanocomposite metal-oxides with enhanced catalytic performance in thermal decomposition of ammonium perchlorate. *J. Alloys Compd.* **2020**, *832*, 154837. https://doi.org/10.1016/j.jallcom.2020.154837
7. Shu, Y.; Chen, H.; Chen, N.; Duan, X.; Zhang, P.; Yang, S.; Bao, Z.; Wu, Z.; Dai, S. A principle for highly active metal oxide catalysts via NaCl-based solid solution. *Chem.* **2020**, *6*, 1723-1741. https://doi.org/10.1016/j.chempr.2020.04.003
8. Alavi, M.; Rai, M. Topical delivery of growth factors and metal/metal oxide nanoparticles to infected wounds by polymeric nanoparticles: an overview. *Expert Rev. Anti Infect. Ther.* **2020**, *18*, 1021-1032. https://doi.org/10.1080/14787210.2020.1782740
9. Derakhshankhah, H.; Jafari, S.; Sarvari, S.; Barzegari, E.; Moakedi, F.; Ghorbani, M.; Varnamkhasti, B.S.; Jaymand, M.; Izadi, Z.; Tayebi, L. Biomedical applications of zeolitic nanoparticles, with an emphasis on medical interventions. *Int. J. Nanomed.* **2020**, *15*, 363. https://dx.doi.org/10.2147%2FIJN.S234573
10. Sheel, R.; Kumari, P.; Panda, P.K.; Ansari, M.D.J.; Patel, P.; Singh, S.; Kumari, B.; Sarkar, B.; Mallick, M.A.; Verma, S.K. Molecular intrinsic proximal interaction infer oxidative stress and apoptosis modulated in vivo biocompatibility

of P. niruri contrived antibacterial iron oxide nanoparticles with zebrafish. *Environ. Poll.* **2020**, *267*, 115482. https://doi.org/10.1016/j.envpol.2020.115482

11. Lai, R.W.S.; Yung, M.M.N.; Zhou, G.J.; He, Y.L.; Ng, A.M.C.; Djurisic, A.B.; Shih, K.; Leung, K.M.Y. Temperature and salinity jointly drive the toxicity of zinc oxide nanoparticles: a challenge to environmental risk assessment under global climate change. *Environ. Sci. Nano*, **2020**, *7*, 2995-3006. https://doi.org/10.1039/D0EN00467G
12. Wiesmann, N.; Tremel, W.; Brieger, J. Zinc oxide nanoparticles for therapeutic purposes in cancer medicine. *J. Mater. Chem. B*, **2020,** *8*, 4973-4989. https://doi.org/10.1039/D0TB00739K
13. Jaballah, S.; Benamara, M., Dahman, H.; Lahem, D.; Debliquy, M.; El Mir, L. Formaldehyde sensing characteristics of calcium-doped zinc oxide nanoparticles-based gas sensor. *J. Mater. Sci. Mater. Electron*. **2020**, *31*, 8230-8239. https://doi.org/10.1007/s10854-020-03358-y
14. Nayak, S.; Chaudhari, A.; Vaidhun, B. Synthesis, characterization and ameliorative properties of food, formulation and cosmetic additives: Case study of Zinc oxide nanoparticles. *J. Excip. Food Chem.* **2020**, *11*, 79-92.
15. Moghaddas, S.M.T.H.; Elahi, B.; Javanbakht, V. Biosynthesis of pure zinc oxide nanoparticles using Quince seed mucilage for photocatalytic dye degradation. *J. Alloys Compd.* **2020**, *821*, 153519. https://doi.org/10.1016/j.jallcom.2019.153519
16. Abdelhakim, H.K.; El-Sayed, E.R.; Rashidi, F.B. Biosynthesis of zinc oxide nanoparticles with antimicrobial, anticancer, antioxidant and photocatalytic activities by the endophytic *Alternaria tenuissima*. *J. Appl. Microbiol.* **2020**, *128*, 1634-1646. https://doi.org/10.1111/jam.14581

17. Brindhadevi, K.; Samuel, M.S.; Verma, T.N.; Vasantharaj, S.; Sathiyavimal, S.; Saravanan, M.; Pugazhendhi, A.; Duc, P.A. Zinc oxide nanoparticles (ZnONPs)-induced antioxidants and photocatalytic degradation activity from hybrid grape pulp extract (HGPE). *Biocatal. Agric. Biotech.* **2020**, *28*, 101730. https://doi.org/10.1016/j.bcab.2020.101730

18. Awwad, A.M.; Amer, M.W.; Salem, N.M. Abdeen, A.O. Green synthesis of zinc oxide nanoparticles (ZnO-NPs) using Ailanthus altissima fruit extracts and antibacterial activity. *Chem. Int.* **2020**, *6*, 151-159. https://doi.org/10.5281/zenodo.3559520

19. Ahmed, S.; Chaudhry, S.A.; Ikram, S. A review on biogenic synthesis of ZnO nanoparticles using plant extracts and microbes: a prospect towards green chemistry. *J. Photochem. Photobiol. B: Biology*, **2017**, *166*, 272-284. https://doi.org/10.1016/j.jphotobiol.2016.12.011

20. Yuliarto, B.; Septiani, N.L.W.; Kaneti, Y.V.; Iqbal, M.; Gumilar, G.; Kim, M.; Na, J.; Wu, K.C.W.; Yamauchi, Y. Green synthesis of metal oxide nanostructures using naturally occurring compounds for energy, environmental, and bio-related applications. *New J. Chem.* **2019,** *43*, 15846-15856. https://doi.org/10.1039/C9NJ03311D

21. Bernstein, A.M.; Titgemeier, B.; Kirkpatrick, K.; Golubic, M.; Roizen, M.F. Major cereal grain fibers and psyllium in relation to cardiovascular health. *Nutrients* **2013**, *5*, 1471-1487. https://doi.org/10.3390/nu5051471

22. Hou, Q.; Li, Y.; Li, L.; Cheng, G.; Sun, X.; Li, S.; Tian, H. The metabolic effects of oats intake in patients with type 2 diabetes: a systematic review and meta-analysis. *Nutrients* **2015**, *7*, 10369-10387. https://doi.org/10.3390/nu7125536

23. Li, X.; Cai, X.; Ma, X.; Jing, L.; Gu, J.; Bao, L.; Li, J.; Xu, M.; Zhang, Z.; Li, Y. 2016. Short-and long-term effects of wholegrain oat intake on weight management and glucolipid metabolism in overweight type-2 diabetics: a randomized control trial. *Nutrients* **2016**, *8*, 549. https://doi.org/10.3390/nu8090549

24. He, L.X.; Zhao, J.; Huang, Y.S.; Li, Y. The difference between oats and beta-glucan extract intake in the management of HbA1c, fasting glucose and insulin sensitivity: a meta-analysis of randomized controlled trials. *Food funct.* **2016**, *7*, 1413-1428. https://doi.org/10.1039/C5FO01364J

25. Rasane, P.; Jha, A.; Sabikhi, L.; Kumar, A.; Unnikrishnan, V.S. Nutritional advantages of oats and opportunities for its processing as value added foods-a review. *J. Food Sci. Technol.* **2015**, *52*, 662-675. https://doi.org/10.1007/s13197-013-1072-1

26. Emamifar, S.; Abolmaali, S.; Sohrabi, S.M.; Mohammadi, M.; Shahmohammadi, M. Molecular characterization and evaluation of the antibacterial activity of a plant defensin peptide derived from a gene of oat (Avena sativa L.). *Phytochem.* **2021**, *181*, 112586. https://doi.org/10.1016/j.phytochem.2020.112586

27. Sumina, A.V.; Polonsky, V.I.; Shaldaeva, T.M.; Shulbaeva, M.T. Oat talgan as a source of antioxidants. *RUDN J. Agron. Anim. Indus.* **2020**, *15*, 19-29. https://doi.org/10.22363/2312-797X-2020-15-1-19-29

28. Oraby, H.F.; El-Tohamy, M.F.; Kamel, A.M.; Ramadan, M.F. Changes in the concentration of avenanthramides in response to salinity stress in CBF3 transgenic oat. *J. Cereal Sci*. **201**7, *76*, 263-270. https://doi.org/10.1016/j.jcs.2017.06.010

29. Al-Tamimi, S.A. Biogenic green synthesis of metal oxide nanoparticles using oat biomass for ultrasensitive modified polymeric sensors. *Green Chem. Lett. Rev.* **2021**, *14*, 165-178. https://doi.org/10.1080/17518253.2021.1895326

30. Abdpour, S.; Kowsari, E.; Moghaddam, M.R.A.; Schmolke, L.; Janiak, C. Mil-100 (Fe) nanoparticles supported on urchin like Bi2S3 structure for improving photocatalytic degradation of rhodamine-B dye under visible light irradiation. *J. Solid State Chem.* **2018**, *266*, 54-62. http://dx.doi.org/10.1016/j.jssc.2018.07.006

31. Adnan, M.M.; Julkapli, N.M.; Amir, M.N.I.; Maamor, A. Effect on different TiO_2 photocatalyst supports on photodecolorization of synthetic dyes: a review. *Int. J. Environ. Sci. Technol.* **2019**, *16*, 547-566. http://dx.doi.org/10.1007/s13762-018-1857-x

32. Zhang, G.; Zhang, X.; Meng, Y.; Pan, G.; Ni, Z.; Xia, S.; Layered double hydroxides-based photocatalysts and visible-light driven photodegradation of organic pollutants: a review. *Chem. Eng. J.* **2020**, *392*, 123684. http://dx.doi.org/10.1016/j.cej.2019.123684

33. Zhu, X.; Wu, G.; Wang, C.; Zhang, D.; Yuan, X. A miniature and low-costelectrochemical system for sensitive determination of rhodamine B. *Measurement* **2018**, *120*, 206–212. http://dx.doi.org/10.1016/j.measurement.2018.02.014.

34. Wang, Y.; Song, H.; Chen, J.; Chai, S.; Shi, L.; Chen, C.; Wang, Y.; He, C. A novel solar photo-Fenton system with self-synthesizing H_2O_2: Enhanced photo-induced catalytic performances and mechanism insights. *Appl. Surf. Sci.* **2020**, *512*, 145650. http://dx.doi.org/10.1016/j.apsusc.2020.145650.

35. Sarkhosh, M.; Sadani, M.; Abtahi, M.; Azarpira, H.; Alidadi, H.; Atafar, Z.; Rezaei, S.; Mohseni, S.M.; Vaezi, N.; Fakhri, Y.; Keramati, H. 2019. Photo-biological degradation of Bisphenol A, UV/ZnO/Iodide process at the center of biological reactor. *J. Photochem. Photobiol. A: Chem.* **2019**, *374*, 115-124. http://dx.doi.org/10.1016/j.jphotochem.2019.01.040.

36. Cao, H.; Zhang, W.; Wang, C.; Liang, Y. Sonochemical degradation of poly-and perfluoroalkyl substances-a review. *Ultrason. Sonochem.* **2020**, 105245. http://dx.doi.org/10.1016/j.ultsonch.2020.105245

37. Sonia, S.; Ruckmani, K.; Sivakumar, M. Antimicrobial and antioxidant potentials of biosynthesized colloidal zinc oxide nanoparticles for a fortified cold cream formulation: a potent nanocosmeceutical application. *Mater. Sci. Eng. C* **2017**, *79*, 581-589. https://doi.org/10.1016/j.msec.2017.05.059

38. Ashajyothi, C.; Harish, K.H.; Dubey, N.; Chandrakanth, R.K. Antibiofilm activity of biogenic copper and zinc oxide nanoparticles-antimicrobials collegiate against multiple drug resistant bacteria: a nanoscale approach. *J. Nanostruct. Chem.* **2016**, *6*, 329-341. https://doi.org/10.1007/s40097-016-0205-2

39. Christy, S.R.; Priya, L.S.; Durka, M.; Dinesh, A.; Babitha, N.; Arunadevi, S. Simple combustion synthesis, structural, morphological, optical and catalytic properties of ZnO nanoparticles. *J. Nanosci. Nanotechnol.* **2019**, *19*, 3564-3570. https://doi.org/10.1166/jnn.2019.16141

40. Mohammadian, M.; Es'haghi, Z.; Hooshmand, S. Green and chemical synthesis of zinc oxide nanoparticles and size evaluation by UV–vis spectroscopy. *J. Nanomed. Res.* **2018**, *7*, 00175. http://dx.doi.org/10.15406/jnmr.2018.07.00175

41. Patil, B.N.; Taranath, T.C. *Limonia acidissima* L. leaf mediated synthesis of zinc oxide nanoparticles: a potent tool against Mycobacterium tuberculosis. *Int. J. Mycobacteriol.* **2016**, *5*, 197-204. https://doi.org/10.1016/j.ijmyco.2016.03.004

42. Goyal, M.; Singh, M. Size and shape dependence of optical properties of nanostructures. *Appl. Phys. A* **2020**, *126*, 1–8. https://doi.org/10.1007/s00339-020-3327-9

43. Ramesh, M.; Anbuvannan, M.; Viruthagiri, G.J.S.A.P.A.M. Green synthesis of ZnO nanoparticles using Solanum nigrum leaf extract and their antibacterial activity. *Spectrochim. Acta Part A* **2015**, *136*, 864-870. https://doi.org/10.1016/j.saa.2014.09.105

44. Sathyavathi, R.; Krishna, M.B.; Rao, S.V.; Saritha, R.; Rao, D.N. Biosynthesis of silver nanoparticles using Coriandrum sativum leaf extract and their application in nonlinear optics. *Adv. Sci. Lett.* **2010**, *3*, 138-143. https://doi.org/10.1166/asl.2010.1099

45. Stani, C.; Vaccari, L.; Mitri, E.; Birarda, G. FTIR investigation of the secondary structure of type I collagen: New insight into the amide III band. *Spectrochim. Acta Part A Mol. Biomol. Spec.* **2020**, *229*, 118006. https://doi.org/10.1016/j.saa.2019.118006

46. Sirelkhatim, A.; Mahmud, S.; Seeni, A.; Kaus, N.H.M.; Ann, L.C.; Bakhori, S.K.M.; Hasan, H.; Mohamad, D. Review on zinc oxide nanoparticles: antibacterial activity and toxicity mechanism. *Nano-micro Lett.* **2015**, *7*(3), pp.219-242. https://doi.org/10.1007/s40820-015-0040-x

47. Verma, S.K.; Jha, E.; Panda, P.K.; Thirumurugan, A.; Suar, M. Biological effects of green-synthesized metal nanoparticles: a mechanistic view of antibacterial

activity and cytotoxicity. *Adv. Nanostruct. Mater. Environ. Remed.* **2019**, *25*, 145-171. https://doi.org/10.1007/978-3-030-04477-0_6

48. Nguyen, T.D.; La, P.P.H.; Cao, M.T. A comparison study of the photocatalytic activity of ZnO nanoparticles for organic contaminants degradation under low-power UV-A lamp. *Adv. Natural Sci. Nanosci. Nanotechnol.* **2020**, *11*, 015005.
49. Barras, A.; Cordier, S.; Boukherroub, R. Fast photocatalytic degradation of rhodamine B over [Mo6Br8 (N3) 6] 2−cluster units under sun light irradiation. *Appl. Cat. B: Environ.* **2012**, *123*, 1-8. https://doi.org/10.1016/j.apcatb.2012.04.006
50. Akir, S.; Barras, A.; Coffinier, Y.; Bououdina, M.; Boukherroub, R.; Omrani, A.D. Eco-friendly synthesis of ZnO nanoparticles with different morphologies and their visible light photocatalytic performance for the degradation of Rhodamine B. *Ceram, Int.* **2016**, *42*, 10259-10265. https://doi.org/10.1016/j.ceramint.2016.03.153
51. Chandekar, K.V.; Shkir, M.; Al-Shehri, B.M.; AlFaify, S.; Halor, R.G.; Khan, A.; Al-Namshah, K.S.; Hamdy, M.S. Visible light sensitive Cu doped ZnO: facile synthesis, characterization and high photocatalytic response. *Mater. Charact.* **2020**, *165*, 110387. https://doi.org/10.1016/j.matchar.2020.110387
52. Maqbool, H.; Visnuvinayagam, S.; Zynudheen, A.A.; Safeena, M.P.; Kumar, S. 2020. Antibacterial Activity of Beetroot Peel and Whole Radish Extract by Modified Well Diffusion Assay. *Int. J. Curr. Microbiol. App. Sci*, **2020,** *9*, 1222-1231. https://doi.org/10.20546/ijcmas.2020.901.135
53. Alarfaj, N.A.; Amina, M.; Al Musayeib, N.M.; El-Tohamy, M.F.; Oraby, H.F.; Bukhari, S.I.; Moubayed, N.M. Prospective of Green Synthesized Oleum cumini

Oil/PVP/MgO Bionanocomposite Film for Its Antimicrobial, Antioxidant and Anticancer Applications. *J. Polym. Environ.* **2020**, *28*, 2108-2124. https://doi.org/10.1007/s10924-020-01755-2

54. Siddhuraju, P.; Manian, S. The antioxidant activity and free radical-scavenging capacity of dietary phenolic extracts from horse gram (Macrotyloma uniflorum (Lam.) Verdc.) seeds. *Food Chem.* **2007**, *105*, 950-958. https://doi.org/10.1016/j.foodchem.2007.04.040

Preprints (www.preprints.org) | NOT PEER-REVIEWED | Posted: 15 December 2021 doi:10.20944/preprints202112.0259.v1

List of Figure Captions

Figure 1: (a) UV-Vis spectrum of green synthesized ZnONPs using oat biomass: The recorded spectrum screened in the wavelength range 200-500 nm, (b) Photoluminescence spectrum of green synthesized ZnONPs using oat biomass

Figure 2: FT-IR spectra of (a) Oat biomass and (b) ZnONPs at wave numbers range 4000-400 cm^{-1} and (c) XRD analysis of ZnONPs synthesized using oat biomass

Figure 3: EDX spectrum of ZnONPs synthesized using oat biomass: The weight % of Zn 69.9 % and O 30.1%, the atomic % of Zn 36.2% and O 63.77%

Figure 4: (a) TEM and (b) SEM images of ZnONPs synthesized using oat biomass

Figure 5: Antibacterial activity of different concentrations of green synthesized ZnONPs using oat biomass against four bacterial stains

Figure 6: Minimum bacteriostatic concentration (µg mL^{-1}) of the green synthesized ZnONPs using oat biomass against (a) *P. aeruoginosa* and (b) *E.coli* : The data calculated as mean ± SD after triplicate studies

Figure 7: The possible mechanism of antibacterial effect of ZnONPs green synthesized ZnONPs using oat biomass against

Figure 8: SEM images of (A) *P. aeruoginosa* and (B) *E.coli*: (a, d) control, (b,e) the cells treated with oat biomass and (c,f) the cells treated with ZnONPs and the changes in shape

Preprints (www.preprints.org) | NOT PEER-REVIEWED | Posted: 15 December 2021 doi:10.20944/preprints202112.0259.v1

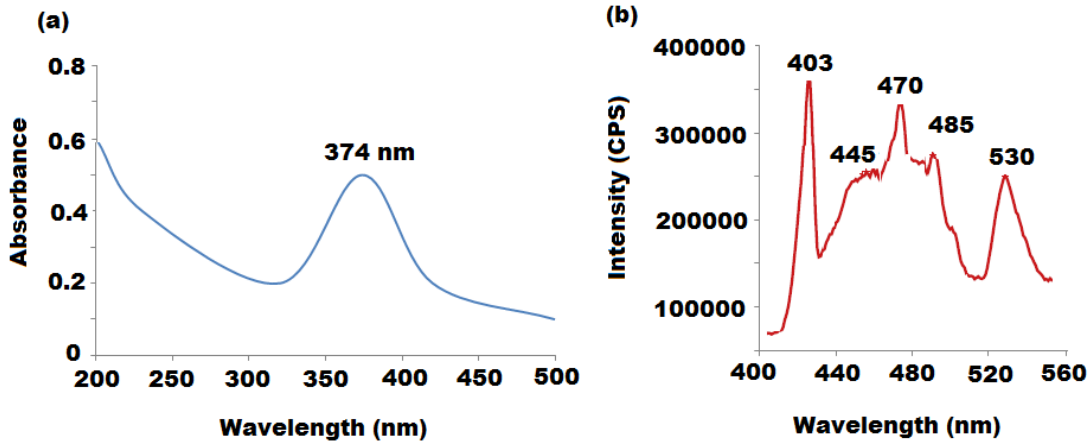

Figure 1: (a) UV-Vis spectrum of green synthesized ZnONPs using oat biomass: The recorded spectrum screened in the wavelength range 200-500 nm, (b) Photoluminescence spectrum of green synthesized ZnONPs using oat biomass

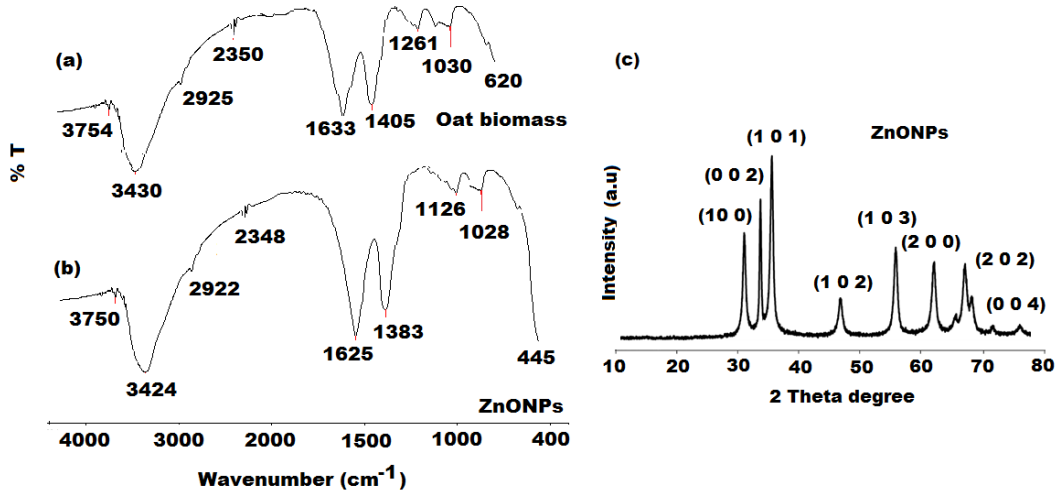

Figure 2: FT-IR spectra of (a) Oat biomass and (b) ZnONPs at wave numbers range 4000-400 cm^{-1} and (c) XRD analysis of ZnONPs synthesized using oat biomass

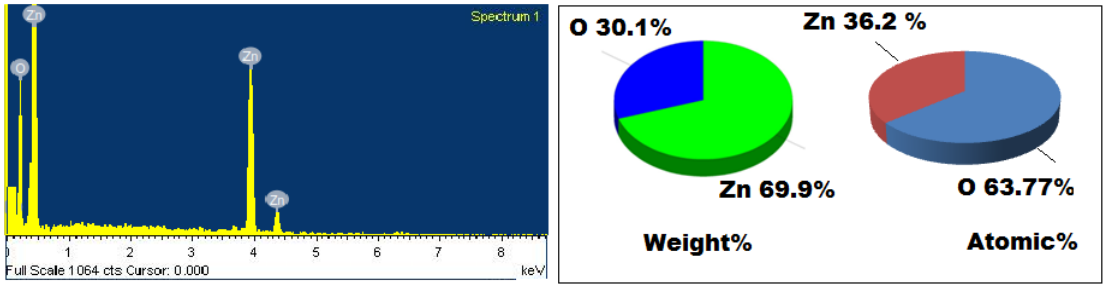

Figure 3: EDX spectrum of ZnONPs synthesized using oat biomass: The weight % of Zn 69.9 % and O 30.1%, the atomic % of Zn 36.2% and O 63.77%

Preprints (www.preprints.org) | NOT PEER-REVIEWED | Posted: 15 December 2021 doi:10.20944/preprints202112.0259.v1

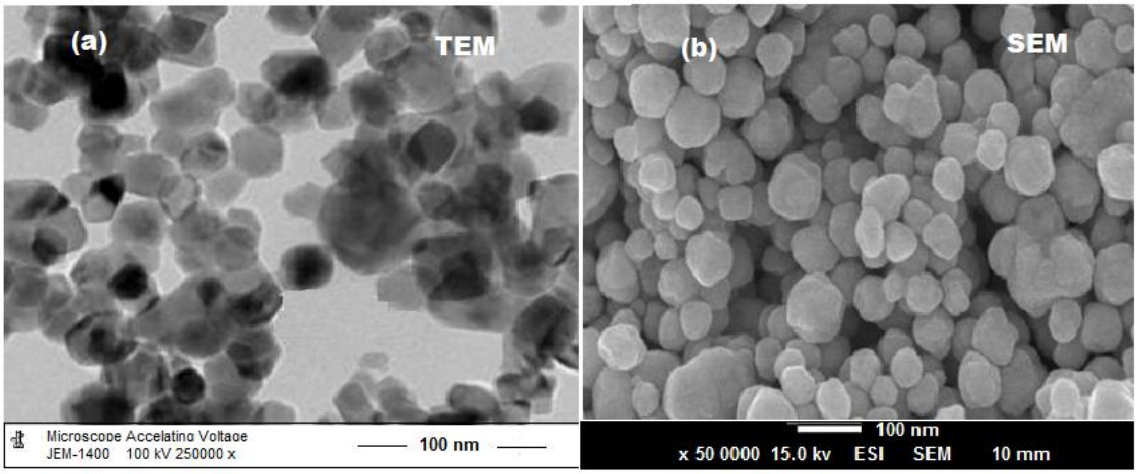

Figure 4: (a) TEM and (b) SEM images of ZnONPs synthesized using oat biomass

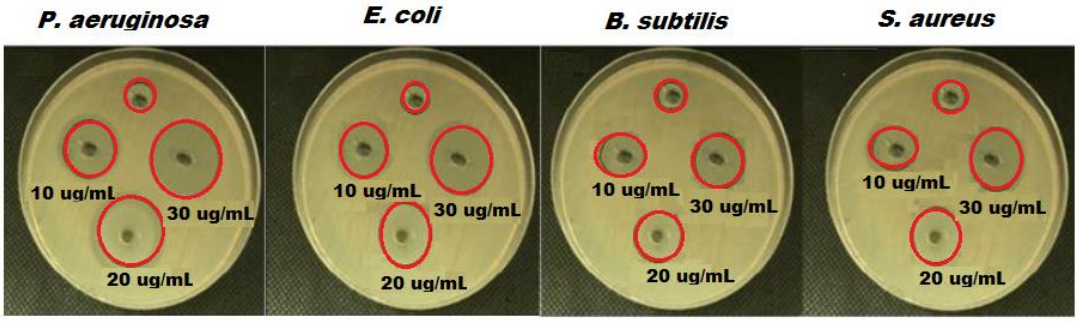

Figure 5: Antibacterial activity of different concentrations of green synthesized ZnONPs using oat biomass against four bacterial stains

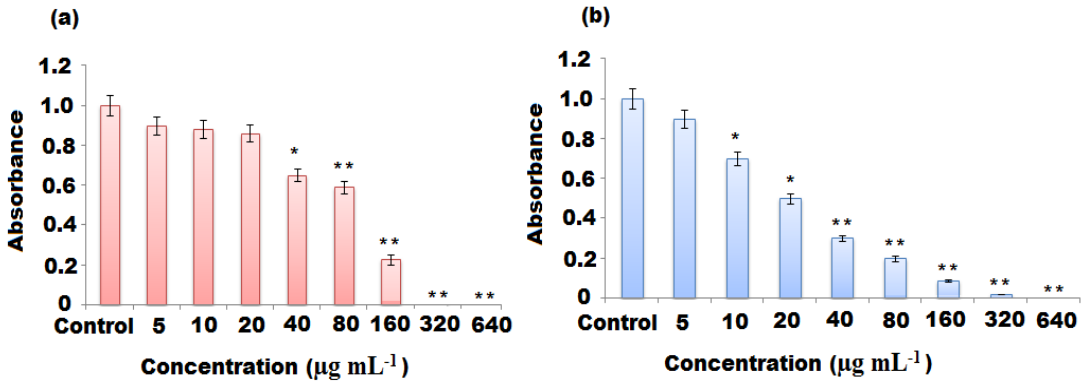

Figure 6: Minimum bactericidal concentration (µg mL^{-1}) of the green synthesized ZnONPs using oat biomass against (a) *P. aeruginosa* and (b) *E.coli*: The data calculated as mean ± SD after triplicate studies

Preprints (www.preprints.org) | NOT PEER-REVIEWED | Posted: 15 December 2021 doi:10.20944/preprints202112.0259.v1

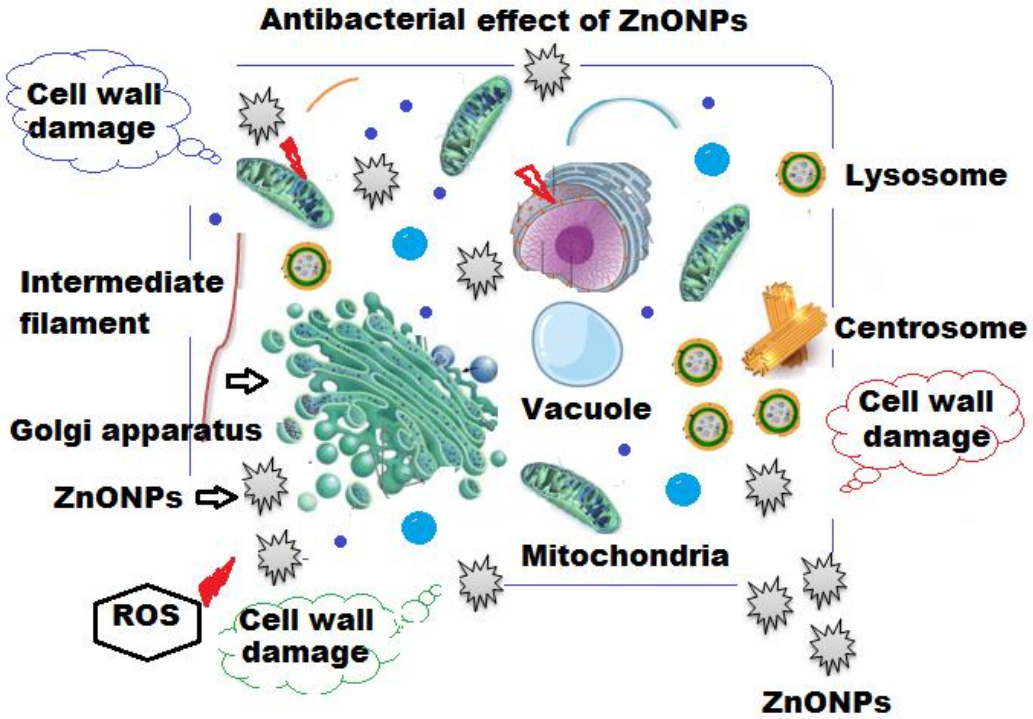

Figure 7: The possible mechanism of antibacterial effect of ZnONPs green synthesized ZnONPs using oat biomass against

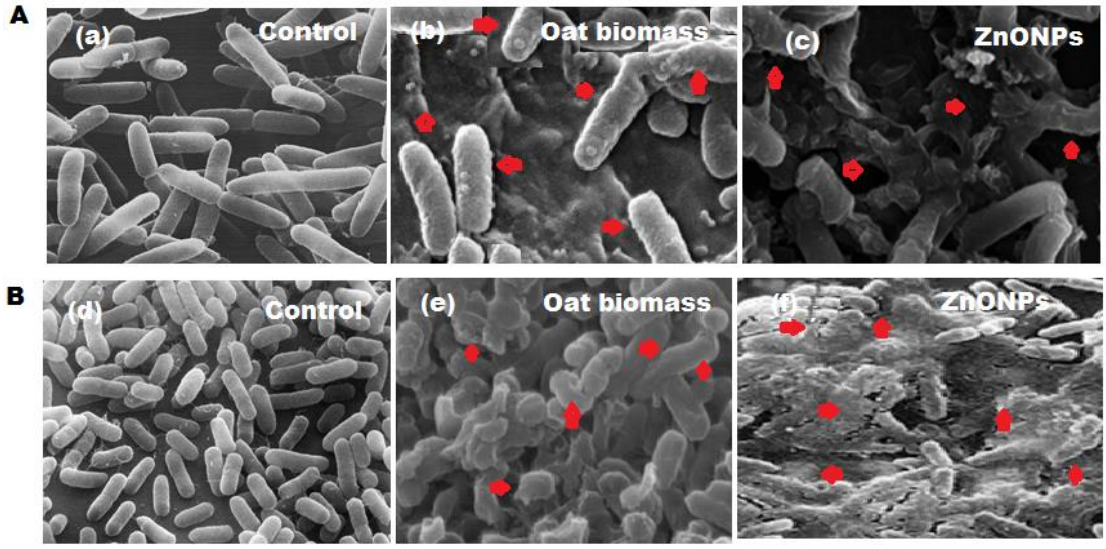

Figure 8: SEM images using 15 kV and magnification 24,000 x of (A) *P. aeruginosa* and (B) *E.coli*: (a, d) control, (b, e) the cells treated with oat biomass and (c, f) the cells treated with ZnONPs and the changes in shape

Preprints (www.preprints.org) | NOT PEER-REVIEWED | Posted: 15 December 2021 doi:10.20944/preprints202112.0259.v1

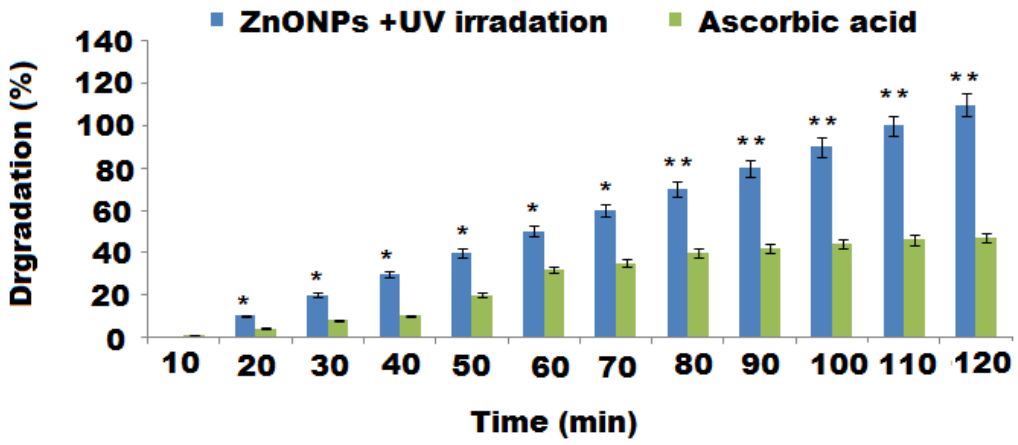

Figure 9: The photocatalytic effect of ZnONPs calculated as % of RB dye degradation in the presence of UV irradiation with respect to ascorbic acid as control: * and ** ($p < 0.05$)

Table 1: Antibacterial effect of ZnONPs synthesized using oat biomass on four different bacterial stains

Bacterial strains	Inhibition zone (mm) at different concentrations of ZnONPs (oat biomass)			Positive control
	10 µg mL^{-1}	20 µg mL^{-1}	30 µg mL^{-1}	
P. aeruginosa	14	15	17	17
E. coli	13	16	16	16
B. subtilis	8	11	11	13
S. aureus	10	10	12	18

Table 2: Least bactericidal potential of ZnONPs synthesized using oat biomass on *P. aeruginosa, E.coli, B. subtilis and S. aureus*

Sample concentration µg mL^{-1}	CFU mL^{-1}			
	P. aeruoginosa	*E. coli*	*B. subtilis*	*S. aureus*
Control	TNTC	TNTC	TNTC	TNTC
5	TNTC	TNTC	TNTC	TNTC
10	TNTC	TNTC	TNTC	TNTC
20	TNTC	TNTC	TNTC	TNTC
40	TNTC	TNTC	TNTC	TNTC
80	TNTC	TNTC	TNTC	TNTC
160	2×10^2	3×10^3	5×10^5	4×10^4
320	NIL	2×10^2	245	135
640	NIL	NIL	5	2

Preprints (www.preprints.org) | NOT PEER-REVIEWED | Posted: 15 December 2021 doi:10.20944/preprints202112.0259.v1

Table 3: The data obtained from DPPH and ABTS scavenging activity of oat biomass and ZnONPs in comparison of ascorbic acid as control

Samples	DPPH radical scavenging effect			ABTS radical scavenging effect		
	Conc. µg mL^{-1}	Scavenging (%)	IC_{50} µg mL^{-1}	Conc. µg mL^{-1}	Scavenging (%)	IC_{50} µg mL^{-1}
Oat biomass	25	26.37±0.67	1.65±0.05	25	35.12±0.24	1.63±0.07
	75	32.92±0.14		75	45.36±0.38	
	100	53.64±0.25		100	45.36±0.47	
ZnONPs	25	58.37±0.67	0.88±0.03	25	53.14±0.53	0.73±0.05
	75	62.18±0.18		75	59.36±0.25	
	100	67.64±0.12		100	71.56±0.84	
Ascorbic acid	25	51.36±0.42	0.35±0.07	25	52.62±0.58	0.27±0.02
	75	56.85±0.73		75	57.36±0.32	
	100	73.00±0.35		100	72.54±0.83	